

Performance of copper doped zinc oxide nanoparticles synthesized through solid state reaction route for humidity sensing device

V. Rajpoot^{a,*}, B. Das^a, V. Rajput^b, A. S. Verma^{c,d,*}

^a*Advanced Materials Research Lab, Department of Physics, University of Lucknow, Lucknow, (226007) India*

^b*Department of Physics, Government Girls Inter College Huzoorpur, Bahraich, (271872) India*

^c*Division of Research and Innovation, School of Applied and Life Sciences, Uttarakhand University, Dehradun, (248007) India*

^d*University Centre for Research & Development, Department of Physics, Chandigarh University, Mohali, Punjab (140413) India*

In the current study, the moisture-sensing properties of three Copper (1%) doped Zinc Oxide nanomaterials, CZ-1, CZ-2, and CZ-3, are examined. These substances were created by solid-state interactions involving Cu₂O and ZnO, CuO and ZnO, and, separately, Cu and ZnO. After four hours of annealing at 700°C for each of the three pellet samples, humidity-sensing tests were conducted. Throughout the whole range of relative humidity percent (15-90%RH) at room temperature, it was observed that the electrical resistance of all three nanomaterials reduced steadily. Powder x-ray diffractometer and scanning electron microscopy analyses were performed on the nanomaterial pellets to determine their crystallinity, structural phases (gross crystal structure), and surface morphology. Both the Scherer's approach and the Williamson and Hall's method were used to determine the crystallite size of the three samples, CZ-1, CZ-2, and CZ-3. The CZ-3 sample annealed at 700°C had the lowest crystallite size (36 nm) and the highest humidity sensitivity of the three samples.

(Received September 3, 2023; Accepted January 10, 2024)

Keywords: ZnO, SEM, XRD, Hysteresis, Aging

1. Introduction

A humidity sensor is a significant electrical gadget that has use in both industrial settings and many types of study. Applications for humidity sensors based on semiconductor metal oxides, such as TiO₂, WO₃, SnO₂, In₂O₃, ZnO, Al₂O₃, Bi₂O₃, etc., have been seen recently in the field of solid-state humidity sensors. For high sensitivity, strong selectivity, quick recovery, and reaction time, a humidity sensor typically needs three decades of quantitative research. [1-3].

For industrial and other uses, ZnO is a versatile material. For optoelectronic devices, photodiodes, optical modulator waveguides, solar cells, fluorescence, high luminous transmittance, and other electronic applications, it is an excellent choice because to its exceptional features, such as a direct band gap of 3.37 eV. Its usual characteristics, straight band gap, transparency in the visual range, and lack of toxicity make it one of the most valuable oxides. Materials made from metal oxides like copper oxide (CuO) and zinc oxide (ZnO) are excellent choices for humidity sensor devices. A p-type semiconductor material with a small band gap (1.7 eV) is copper oxide (CuO) [4]. When Cu's behaviour as an acceptor impurity in n-type ZnO was discovered, it was decided to introduce copper oxide because it significantly changed the electrical and optical characteristics of ZnO [5-7]. Rajput et al [8] have studied and suggested that the humidity sensitivity of the nanocomposite CuO-ZnO prepared by the solid-state reaction route increased as the doping % increased. By using aqueous fruit extracts of Myristica fragrans, Faisal et al. [9] have created bioaugmented zinc oxide nanoparticles. Synthesized nanoparticles were tested for their potential antibacterial, antidiabetic, antioxidant, antiparasitic, and larvicidal characteristics, and it

* Corresponding authors: ajay_phy@rediffmail.com

<https://doi.org/10.1525/JOR.2024.201.57>

was discovered that they were quite effective against bacterial strains coated in antibiotics. ZnO-NPs made from *Myristica fragrans* may be used as viable candidates for biomedical and environmental applications because of their eco-friendly synthesis, nontoxicity, and biocompatible nature. The zinc-tolerant *Lactobacillus plantarum* TA4 cell-biomass (CB) and supernatant (CFS) have been used by Yusof et al. [10] as a potential nanofactory to create ZnO NPs. According to their explanation, biosynthesized ZnO NPs had antibacterial activity against pathogenic bacteria in a concentration-dependent manner and demonstrated biocompatibility with the Vero cell line at certain doses. All things considered, *L. plantarum* TA4's CFS and CB might be utilized as a nanofactory for the biological manufacture of ZnO NPs. Easy polyol-mediated ZnO nanoparticle production, characterization, and antibacterial properties against pathogenic microbes have all been studied by Mahamuni et al. [11]. By 3 hours of refluxing zinc acetate dihydrate in diethylene glycol, they created ZnO nanoparticles with the smallest size (~15 nm), which showed remarkable antibacterial and antibiofilm activity and could potentially replace current biomedical treatments. The environmentally friendly production, characterization, and use of ZnO nanoparticles for photocatalysis and microbiological applications have been discussed by Ashwini et al. [12]. The bark extract of *Acacia caesia* (L.) Willd was combined with zinc nitrate hexahydrate to create ZnO nanoparticles in a green manner. Significant photocatalytic activity was demonstrated by the synthesised nanoparticles (methyl blue under UV illumination). The photocatalytic degradation of the model pollutant Methyl Blue allowed for the analysis of the rate constants and correlation coefficients that were altered by the presence of nanoparticles. Studies on antifungal (*Aspergillus niger*, *Candida albicans*), antibacterial (*Escherichia coli*, *Staphylococcus aureus*), and anti-inflammatory (COX test) characteristics were also conducted. The nanoparticles were created using an economical and environmentally friendly process. The research widens the scope of the fields of nanotechnology, biosensors, and water treatment.

2. Synthesis

2.1. Fabrication of nanocomposites (sensing elements)

The nanocomposite ZnO-Cu₂O (CZ-1), CuO-ZnO (CZ-2), and Cu-ZnO (CZ-3) have been prepared by the solid-state reaction method. The starting material is ZnO (Qualizens, 99.99% pure) and CuO, Cu₂O, and Cu powder (Loba Chemie, 99.9%). 10-weight % glass powder has been used as a binder. Pellets samples have been prepared with compositions of 1 weight % of CuO doped ZnO, Cu₂O doped ZnO and Cu doped ZnO and mixed uniformly by using glaze mortar and pestle for 8 hours. The resultant powder was pressed into pellets under a pressure of 390 MPa. All three pellet samples were annealed at 700°C for four hours and thereafter humidity-sensing studies were carried out. It has been observed that the resistance of the sample continuously decreases when the relative humidity in the chamber increases to the range of 15% to 90% RH at room temperature.

2.2. Characterization

2.2.1. Scanning electron microscope (SEM)

By using a Scanning Electron Microscope (SEM), the surface morphology of the pellet samples was examined.

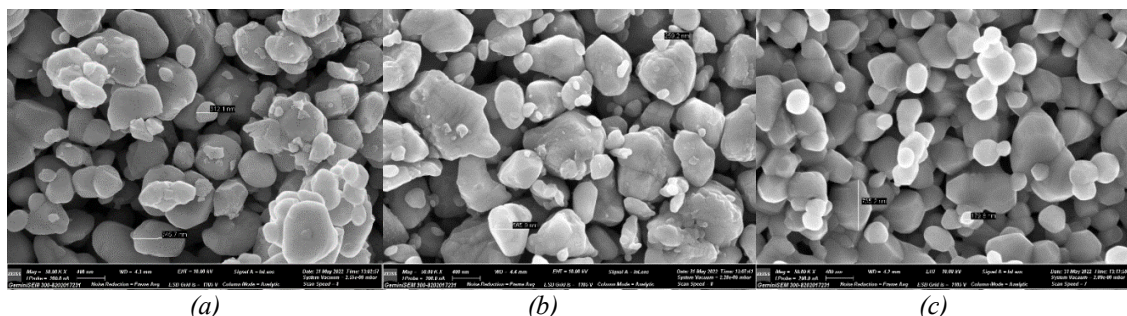


Fig. 1. Surface morphology of (a) CZ-1, (b) CZ-2 and (c) CZ-3 Samples.

Table 1. Values of grain size for the sensing elements at 700 C temperatures.

Sample Cu ₂ O-ZnO (CZ-1)	528.6 nm
Sample CuO-ZnO (CZ-2)	412.5 nm
Sample Cu-ZnO (CZ-3)	457.5 nm

Before SEM examination, 10 nm thick gold metal sheets were sputtered by DC onto the surfaces of the pellets. The surface morphology of sensing material in the form of a pellet has been investigated. Figure 1(a), 1(b) and 1(c) reveals SEM of samples (CZ-1), (CZ-2) and (CZ-3) in the form of pellet at temperature 700°C respectively. We have calculated average grain size of samples CZ-1, CZ-2 and CZ-3 from SEM micrographs and are shown in Table 1.

2.2.2. X-ray diffraction pattern

In order to get a detailed understanding of the crystallinity, structural phases, and gross crystal structure of the produced nanocomposite materials, an X-ray diffractometer was used. The CuKa source had a wavelength of 1.54060. The typical X-ray diffraction (XRD) patterns for the samples (CZ-1), (CZ-2), and (CZ-3) are shown in Figures 2(a), 2(b), and 2(c), respectively.

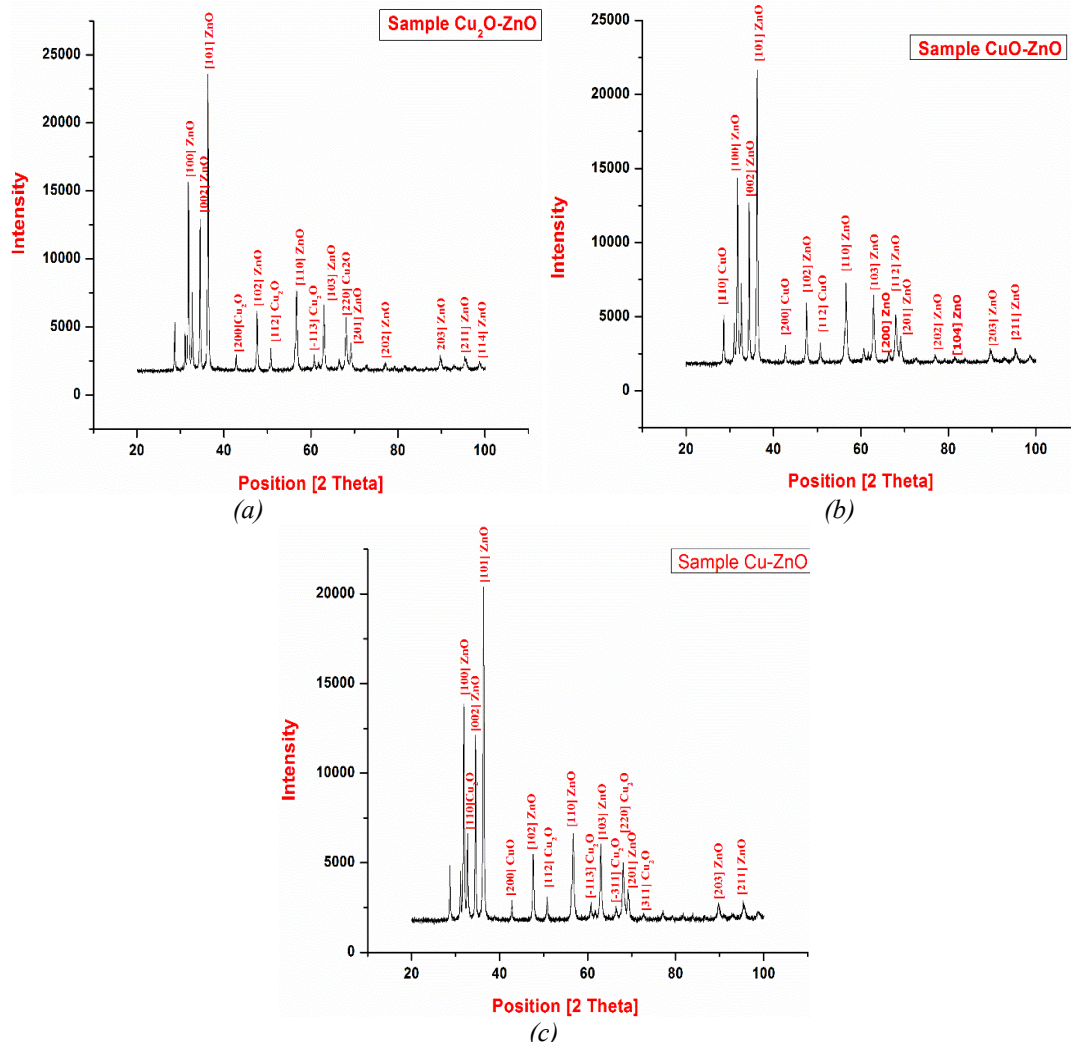


Fig. 2. XRD-Pattern of (a) CZ-1, (b) CZ-2 and (c) CZ-3 Samples.

The measured d-spacing values from Bragg's law are nearly comparable to the d-spacing values of samples (CZ-1), (CZ-2), and (CZ-3) from JCPDS cards. In order to estimate the average crystalline size of the samples, the Williamson and Hall (W-H) method was used along with the Debye-Scherer formula [13-15]. In addition to strain related to lattice distortions brought on by lattice defects, decreased crystallite size also contributes to the widening of x-ray diffraction peaks. Lorentzian broadening profiles are predicted by Williamson and Hall for both large and small strains. This leads them to draw the following relationship between the lattice microstrain (ϵ) and the average crystallite size (D),

$$\beta \cos\theta = k\lambda/D + 4\epsilon \sin\theta \quad (1)$$

Here, β is full-width half maxima; λ is radiation's wavelength; k is constant, and θ is peak position. When $\beta \cos\theta$ vs $4\sin\theta$ is plotted and based on the intercept and slope of the straight line, we have estimated crystallite size and lattice strain. These Williamson and Hall (W-H) plots for samples CZ-1, CZ-2, and CZ-3 are shown in figure 3(a), 3(b), and 3(c) respectively. A W-H plot for samples CZ-1, CZ-2, and CZ-3 and the crystallite size calculated using Debye-Scherer's formula are provided in Table 2. The crystallite size calculated by W-H analysis is more accurate [16].

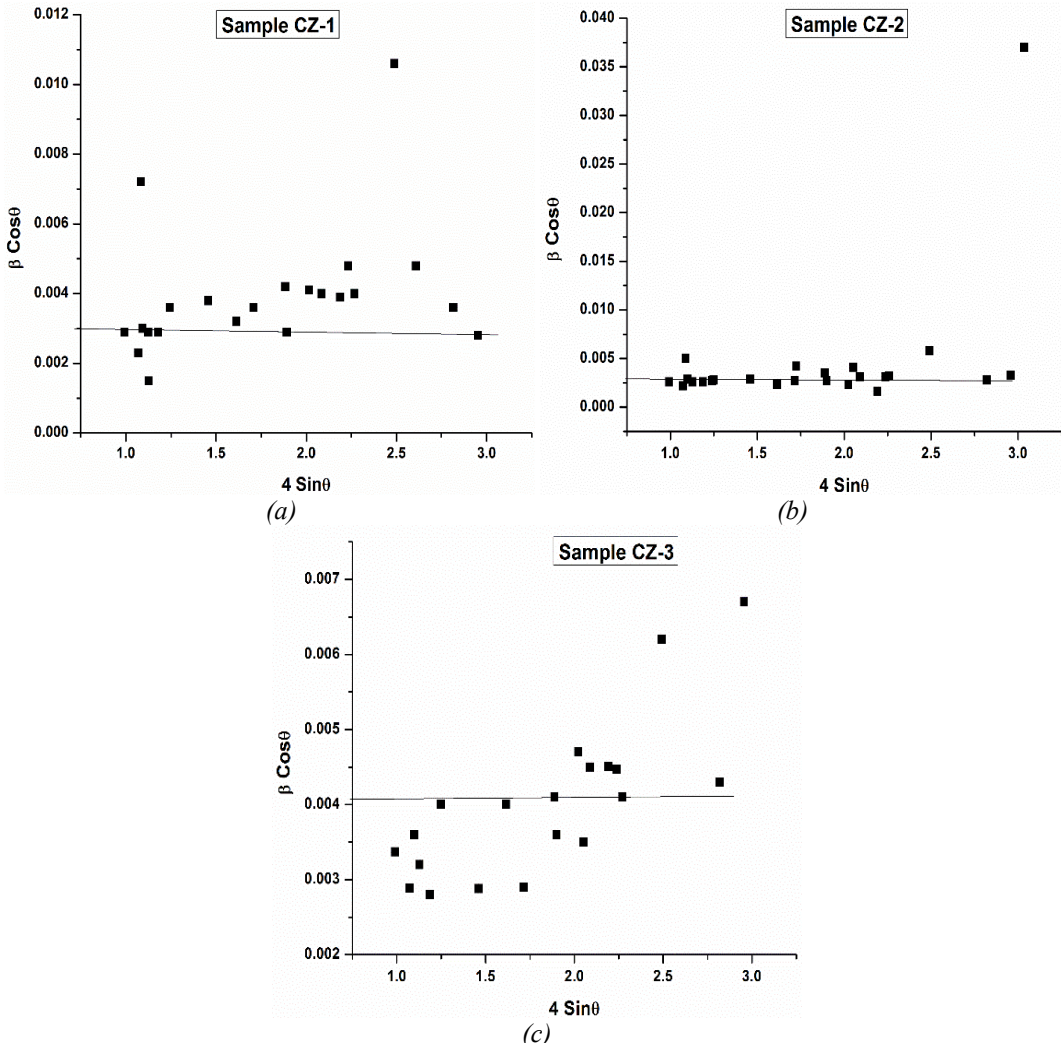


Fig. 3. Williamson and Hall (W-H) plots of (a) CZ-1, (b) CZ-2 and (c) CZ-3 Samples.

Table 2. Values of crystallite size for all the sensing elements.

Sensing element	crystallite size (nm)	
	From Scherer's formula	From W-H Graph
Sample Cu ₂ O-ZnO (CZ-1)	48.43	51.33
Sample CuO-ZnO (CZ-2)	40.72	38.5
Sample Cu-ZnO (CZ-3)	36.41	36.66

2.3. Humidity sensitivity measurement

After annealing, measurements were performed in a controlled humidity chamber [17,18]. A standard hygrometer (Huger, Germany, 1% RH) and thermometer (1°C) are put inside the humidity chamber for calibration. Using a copper electrode, the resistance of the pellet has been conventionally measured to its cross-section. Both a dehumidifier and a humidifier were employed, using saturated solutions of potassium hydroxide and sulphate, respectively. Resistance variation has been seen in relation to variations in relative humidity. A digital multimeter was used to test the samples' resistance (sinometer, $\pm .001\text{M}\Omega$, Model: VC-9808). A conventional hygrometer and thermometer were used to measure the relative humidity (Huger, Germany, 1% RH). Throughout this procedure, the chamber's temperature stayed constant throughout the experiment. The resistance of the pellet has been measured using a copper electrode. The Cu electrode had a square form and sides that measured 2 cm long. A Cu electrode-pellet-equipped conductivity measurement holder was used to place the prepared pellet inside.

The chamber was then dried out using a potassium hydroxide dehumidifier to a relative humidity of 10%. The least count for the hygrometer and thermometer, respectively, is 1% RH and 1°C. The pellet's resistance has been quantified as normal to its cylindrical surface. A two-probe approach was used to assess the electrical resistance of the pellet-shaped sensor devices at various relative humidity levels. The resistance of the pellet reduced across the full range of humidity when it was subjected to humidity inside a specially created controlled humidity chamber, as measured by relative humidity (% RH) namely, 15% to 90%. The sensor material pellet underwent four hours of consecutive annealing at 700°C in an electric furnace. The pellet was exposed to humidity following each phase annealing, and changes in resistance with humidity were noted. The change in resistance (ΔR) of the sensing element per unit change in percentage RH has been used to quantify the sensitivity of a humidity sensor.

3. Results and discussion

3.1. Humidification Graphs

Variation in resistance with the change in relative humidity has been recorded for the samples (CZ-1), (CZ-2), and (CZ-3). All the results are repeatable. Figure 4 depicts the humidity response for the samples (CZ-1), (CZ-2), and (CZ-3).

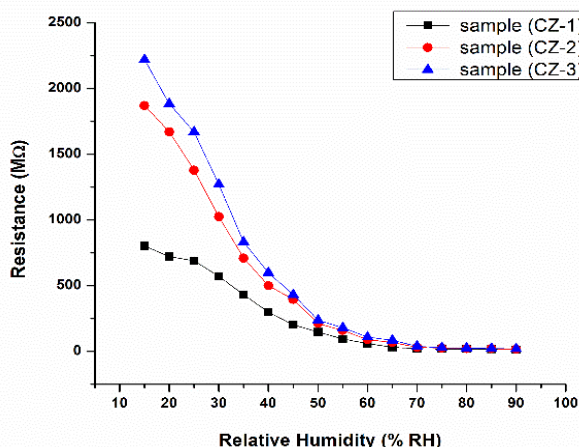


Fig. 4. Humidity response for the samples (CZ-1), (CZ-2), and (CZ-3).

3.2. Humidification and Desiccation Graph: Hysteresis

Hysteresis of all the samples (CZ-1), (CZ-2), and (CZ-3) has been calculated but reported here only for the sample (CZ-3), this sample shows less hysteresis as compared to others. A hysteresis graph in Figure 5 shows that the electrical resistance of CZ-3 varies with both increasing and decreasing cycles of relative humidity.

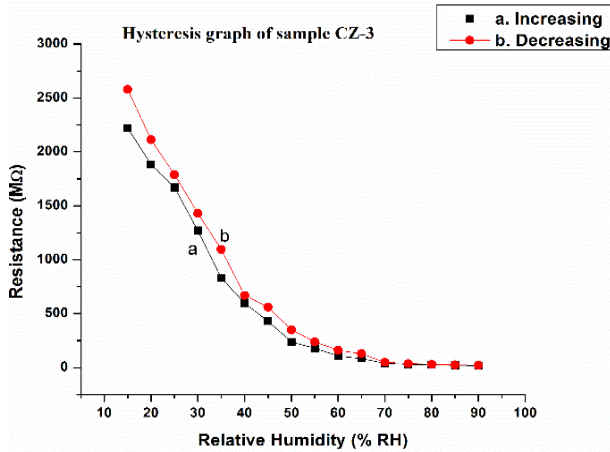


Fig. 5. Hysteresis graph of sample CZ-3

The hysteresis effects are thought to be caused by initial chemisorptions on the surface of the sensing components. Chemically bonded layers cannot be further affected by humidity exposure or removal; they can only be desorbable by thermal means. Hysteresis results from the initial adsorbed water not being completely eliminated throughout the decreasing cycle of % RH. The minimum hysteresis for sample CZ-3 was calculated and found to be $\pm 6\%$ and the average hysteresis for sample CZ-3 is $\pm 19\%$.

3.3. Problem of Aging in Humidity Sensor

Just after humidity treatment, the sensing element samples were maintained in a laboratory environment, and their ability to detect humidity was periodically checked three months later. The humidity control chamber was examined three months later to see if the sensing element had changed with aging and reproduction [17,18]. The results are generally reproducible over different cycles of operation. The repeatability graph for the sensor component CZ-3 is shown in Figure (6). Both the initial growing cycle and the subsequent increasing cycle after three months are depicted combined in this graph. Aging for sample CZ-3 $\pm 7\%$ for 3 months.

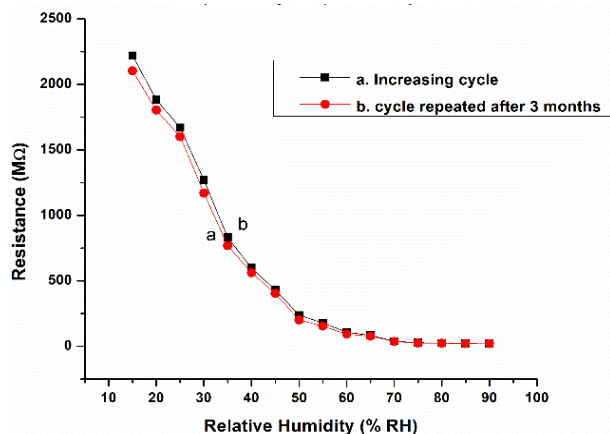


Fig. 6. Repeatability Graph of sample CZ-3

3.4. Sensitivity

The change in resistance (ΔR) of the sensing element per unit change in relative humidity (% RH) is used to characterize a humidity sensor's sensitivity.

$$S = \Delta R / (\Delta \% \text{RH}) \quad \text{M}\Omega / \% \text{RH} \quad (2)$$

The Sensitivity of all the samples CZ-1, CZ-2, and CZ-3 has been calculated and shown in table (3). The sample CZ-3 showed the best results with sensitivity 34.12 MΩ /%RH.

Table 3. Sensitivity of Samples (MΩ /%RH).

Samples	Sensitivity of Samples (MΩ /%RH) over the entire range from 15 to 95 % RH for annealing temperature 700°C		
	a	b	c
Sample CZ-1	10.50	13.81	8.21
Sample CZ-2	24.73	27.94	22.94
Sample CZ-3	29.33	34.12	27.78

^aIncreasing Cycle of Relative Humidity; ^bDecreasing Cycle of Relative Humidity; ^cIncreasing Cycle after three months.

4. Conclusion

The sample with 1 weight % of Cu doped ZnO annealed at 700°C prove to be the best sensing element with a sensitivity of 34.12 MΩ /%RH. This sample manifests lower hysteresis, less effect of aging, and higher reproducibility. As calculated from Scherrer's formula the average crystalline size for the sample CZ-3 is 36.41 nm and according to the SEM micrograph, the grain size is nm. Scherer's formula and Williamson and Hall technique measurements of crystallite size were accurate to within 3% error.

References

- [1] B. C. Yadav, R. Srivastava, C. D. Dwivedi, P. Pramanik, Sensors and Actuators B: Chemical 131 (2008) 216-222; <https://doi.org/10.1016/j.snb.2007.11.013>
- [2] N. L. Hung, Eun Seong Ahn, Hoon Cheol Jung, Hyo Jin Kim, and Do Jin Kim, J Korean Physical Society 57 (2010) 1784-1788; <https://doi.org/10.3938/jkps.57.1784>
- [3] S. Dixit, A. Srivastava, R. K. Shukla, A. Srivastava, J Materials Science: Materials in Electronics 19 (2008) 788-792; <https://doi.org/10.1007/s10854-007-9414-2>
- [4] A. P. Moura, L. S. Cavalcante, J. C. Sczancoski, D. G. Stroppa, E. C. Paris, A. J. Ramirez, José Arana Varela, Elson Longo, Advanced Powder Technology 21 (2010) 197-202; <https://doi.org/10.1016/j.apt.2009.11.007>
- [5] S. T. Jun, and G. M. Choi, J. American Ceramic Society 81 (1998) 695-699; <https://doi.org/10.1111/j.1151-2916.1998.tb02391.x>
- [6] L. Chow, O. Lupan, G. Chai, H. Khallaf, L. K. Ono, B. R. Cuenya, I. M. Tiginyanu, V. V. Ursaki, V. Sontea, A. Schulte, Sensors and Actuators A: Physical 189 (2013) 399-408; <https://doi.org/10.1016/j.sna.2012.09.006>
- [7] R. E. Dietz, H. Kamimura, M. D. Sturge, A. Yariv, Physical Review 132 (1963) 1559; <https://doi.org/10.1103/PhysRev.132.1559>
- [8] V. Rajput, N. Pandey, International J Applied Ceramic Technology 14 (2017) 77-83; <https://doi.org/10.1111/ijac.12620>
- [9] S. Faisal, H. Jan, S.A. Shah, S. Shah, A. Khan, M.T. Akbar, M. Rizwan, F. Jan, A. N.

- Wajidullah, A. Khattak, ACS omega 6 (2021) 9709-9722;
<https://doi.org/10.1021/acsomega.1c00310>
- [10] H. Mohd Yusof, A. Rahman, R. Mohamad, U.H. Zaidan, A.A. Samsudin, Scientific Reports 10, (2020) 19996; <https://doi.org/10.1038/s41598-020-76402-w>
- [11] P. P. Mahamuni, P. M. Patil, M. J. Dhanavade, M. V. Badiger, P. G. Shadija, A. C. Lokhande, R. A. Bohara, Biochemistry and Biophysics Reports, 17 (2019) 71-80;
<https://doi.org/10.1016/j.bbrep.2018.11.007>
- [12] J. Ashwini, T. R. Aswathy, A. B. Rahul, G. M. Thara, A. S. Nair, Catalysts 11 (2021) 1507;
<https://doi.org/10.3390/catal11121507>
- [13] V. K. Pecharsky, PY. Zavalij: New York, NY, Springer (2003).
- [14] M. G. Suranarayana, Norton, X-ray Diffraction: A Practical Approach. New York, Springer Science Business Media, (1998).
- [15] J. R. Patel, M. Cohen, Acta metallurgica 1 (1953) 531-538;
[https://doi.org/10.1016/0001-6160\(53\)90083-2](https://doi.org/10.1016/0001-6160(53)90083-2)
- [16] A. K. Zak, W. H. A. Majid, M. E. Abrishami, R Yousefi, Solid State Sciences 13 (2011) 251-256; <https://doi.org/10.1016/j.solidstatesciences.2010.11.024>
- [17] N. K. Pandey, K. Tiwari, A. Roy, Bulletin of Materials Science 35 (2012) 347-352;
<https://doi.org/10.1007/s12034-012-0290-x>
- [18] I. M., Abdel-Motaleb, P. Navuduri, Y. Z. Yoo, O. Chmaissem, J. H. Song, International J Applied Ceramic Technology 10 (2013) E159-E166l; <https://doi.org/10.1111/ijac.12096>